THE JOURNAL OF PHYSICAL CHEMISTRY B

Article

Cite This: J. Phys. Chem. B 2019, 123, 2679−2686

pubs.acs.org/JPCB

Ab Initio Molecular Dynamics Simulation and Energetics of the Ribulose-1,5-biphosphate Carboxylation Reaction Catalyzed by Rubisco: Toward Elucidating the Stereospecific Protonation Mechanism

Peter L. Cummins,* Babu Kannappan, and Jill E. Gready

John Curtin School of Medical Research, The Australian National University, Canberra ACT 0200, Australia

Supporting Information

ABSTRACT: In the carboxylation reaction catalyzed by ribulose 1,5-bisphosphate (RuBP) carboxylase−oxygenase (Rubisco), which is fundamental to photosynthesis, scission of a C−C bond in the six-carbon gemdiolate intermediate forms a carbanion that must be protonated stereospecifically to form product. It is thought that a conserved lysine side chain (LYS175 in spinach Rubisco), in the immediate vicinity of the carbanion, provides the necessary proton. Here, we endeavor to determine from the electronic-structure calculations whether protonation via this route is energetically possible. The two-dimensional energy surface was mapped to determine the minimum energy path (MEP) using density functional theory (B3LYP) and incorporating basis set superposition and classical (London) dispersion corrections. The potential of mean force (free energy) was then calculated from ab initio molecular dynamics simulations with umbrella sampling in the vicinity of the MEP on the scission−protonation reaction coordinate. MEP calculations were also carried out to evaluate the possibility of an active-site water near the phosphate (P1) of RuBP, with an excess proton positioned at P1, as an alternative facilitator of stereospecific protonation via a classical Grotthuss mechanism. In both cases, the C−C bond scission in the six-carbon intermediate and proton transfer from the donor was found to be concerted and highly asynchronous, without a stable carbanion intermediate. However, the free energy change was unfavorable for direct protonation by the LYS175 side chain. In contrast, the Grotthuss mechanism yielded stable products and an activation energy in good agreement with experiment. It also provides a plausible mechanism for alternative product formed in enzyme mutations at the LYS175 position and is consistent with the observed deuterium isotope effects.

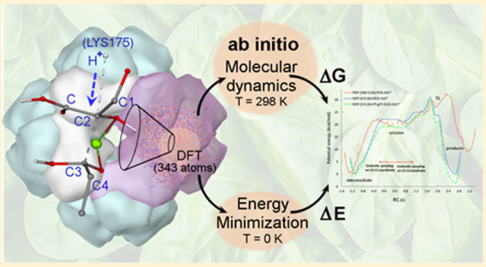

INTRODUCTION

Unravelling the molecular mechanisms of enzymic reactions via computation has three fundamental requirements. First, enough protein (an active-site model) needs to be considered to effectively describe the structure and function of the active site. Second, the practicability and convenience of a methodology suitable to describe the electronic structure with sufficient accuracy needs to be determined. Third, a feasible molecular-dynamics simulation method to represent the thermodynamics of the reaction needs to be identified. Here, we present a fusion of these three requirements into a protocol for investigating a stereospecific protonation mechanism—the final step in the Rubisco carboxylase catalysis. The results reveal that, despite its proximity to the acceptor, the most likely, obvious, active-site residue proton donor (LYS175) does not facilitate the stereospecific protonation, requiring a rethink of an alternative donor, which we suggest here.

The enzyme ribulose 1,5-bisphosphate carboxylase−oxygenase (Rubisco), as the main route for fixation of atmospheric carbon into biological carbon in plant photosynthesis, is an attractive target for re-engineering for improved efficiency and potentially greater crop productivity.[1,2] The successful re-engineering of an enzyme is highly dependent on understanding the catalytic function(s) of Rubisco's totally conserved active-site residues. One such residue, LYS175 (in spinach Rubisco), has been implicated in various phases of the complex multistep reaction catalyzed by Rubisco.[3] In particular, structural analysis reveals that LYS175 is well positioned for the stereospecific protonation that completes the formation of product; consequently, it is considered to be the most likely, if not the only, amino-acid proton donor available to perform this function.[4,5] Our proposed mechanism of Rubisco catalysis is summarized in Figure 1. Here, we focus our attention on the C2−C3 bond scission of the gemdiolate intermediate and stereospecific protonation required to form product; full mechanistic details of the multistep reaction can be found elsewhere.[6] Although we have garnered insights into various aspects of the molecular mechanism from previous computational studies,[6−9] these have often been limited by the accuracy of methodologies used, i.e., those computationally

Received: December 16, 2018
Revised: February 10, 2019
Published: February 26, 2019

DOI: 10.1021/acs.jpcb.8b12088
J. Phys. Chem. B 2019, 123, 2679−2686

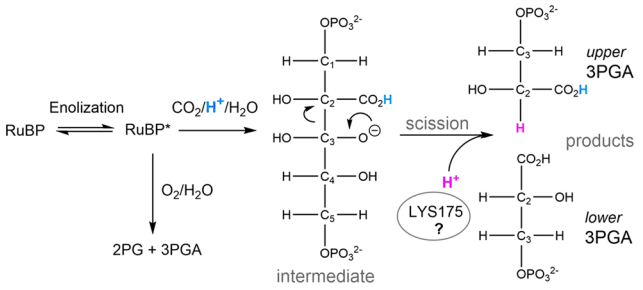

Figure 1. Substrate, D-ribulose 1,5-bisphosphate (RuBP), must first undergo enolization (RuBP*) to bind CO_2 (or O_2 in the oxygenation reaction) at C2. Protonation (blue) of the bound CO_2 facilitates both hydration at C3 (forming the gemdiolate intermediate) and subsequent scission of the C2−C3 bond. In the final phase of the RuBP carboxylation reaction, scission of the C2−C3 bond in the gemdiolate requires stereospecific protonation (magenta) at C2 of the "upper" 3-phospho-D-glyceric acid (3PGA) to produce two (upper plus "lower") molecules of 3PGA. The proton is often assumed to originate from the proximal LYS175. The competing RuBP oxygenation reaction produces one molecule of (lower) 3PGA and one molecule of (upper) 2-phosphoglycolate (2PG).

feasible at the time of the study. Significantly, when investigating enzyme catalysis computationally, it is of interest to know how the free energy, rather than the minimum in potential energy, changes as a function of some reaction coordinate (RC) (the distance between two atoms for example). Of all the free energy methodologies based on molecular dynamics (MD) simulation,[10] the potential of mean force (PMF) is particularly advantageous when the force field used to describe the nuclear motions is evaluated ab initio (i.e., directly from electronic-structure calculations), as the free energy can be obtained efficiently from a probability distribution and, therefore, does not require additional electronic-structure calculations, which can add significantly to the computational cost. Free energy calculations have been carried out previously but at the less consistent, although computationally more efficient, semiempirical QM level.[6] Thus, to better assess the capability of this conserved active-site lysine (LYS175) to protonate C2, we have here computed the PMF based on the electronic-structure calculations using the more accurate, but computationally demanding, Kohn−Sham density functional theory (DFT)[11] for the C2−C3 bond scission and C2 protonation steps in ribulose-1,5-biphosphate (RuBP) carboxylation by Rubisco.

METHODS

As in our previous study of the carboxylation reaction mechanism,[6] we used a fragment model (FM21) to represent the active site of Rubisco. Comprising 343 atoms in total and illustrated in Figure 2, FM21 is based on coordinates from the crystal structure 8RUC (activated spinach Rubisco with Mg^{2+} cofactor and 2-carboxyarabinitol 1,5-bisphosphate, 2CABP reaction-intermediate analogue).[12] In both energy minimization and MD simulations, the added hydrogen atoms (to satisfy valency requirements at the bonds truncated from the enzyme) were fixed in the calculations to mimic enzyme constraints on the active-site geometry. The reaction coordinate was defined in terms of the interatomic C2−C3 and C2−H distances, where H is a proton originating from the side chain of LYS175. The energy-minimized two-dimensional (2D) surface as a function of the C2−C3 and C2−H distances

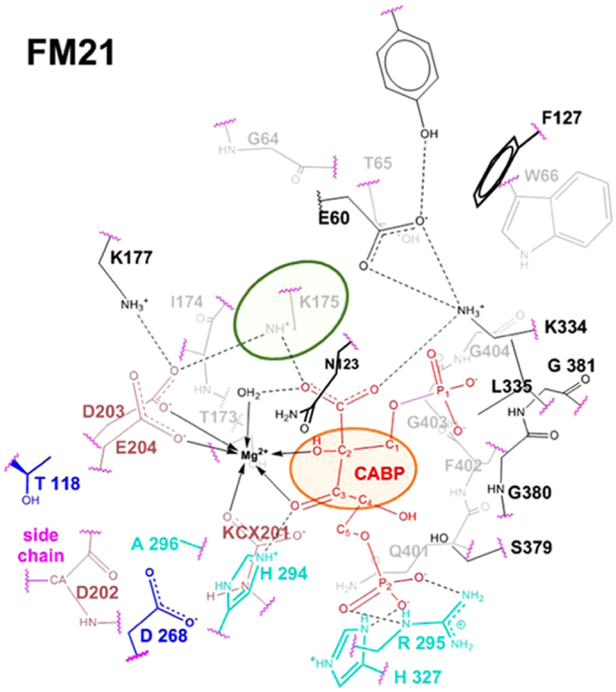

Figure 2. The residues that make up Rubisco active-site model, FM21, are displayed. Where residues overlap visually, residues at the back are shown in gray, and residues at the front are shown in thick black lines. Truncations from enzyme are highlighted as wavy lines in magenta. Some residues, or groups of residues, are shown in color for clarity only, and only the water molecule coordinated to Mg^{2+} is shown. Including all water molecules and link atoms, the model consists of 343 atoms. The proposed proton donor (lysine, K175) and acceptor (C2, shown here for the X-ray structure ligand CABP) in the final step of the reaction are highlighted.

was computed, on a 0.3 au (Bohr) grid (details in the Supporting Information), at the density functional theory (DFT) level using the B3LYP[13−15] exchange−correlation functional with the 6-31G*[16] basis set (B3LYP/6-31G*). We then performed adiabatic (electronic structure within the Born−Oppenheimer approximation) ab initio molecular dynamics (AIMD)[17] simulations, with sampling in the vicinity of the minimum energy pathway (MEP) linking the intermediate and products on the 2D surface. All calculations were carried out using the highly scalable NWChem program.[18] In the AIMD simulations, nuclear motions were integrated using the velocity−Verlet algorithm[19,20] with a time step of 0.5 fs, and the electronic potential was computed at the same level (B3LYP/6-31G*) as in the MEP calculations. The temperature of the AIMD simulations was controlled by the stochastic velocity rescaling thermostat,[21] with a target temperature of 298 K and a relaxation time of 0.02 ps.

PMF simulations are normally implemented with umbrella sampling,[22] as conventional MD simulations typically cannot effectively sample configuration space as they attempt to traverse the energy barriers that may be encountered along the reaction coordinate. In umbrella sampling, an external force is applied to the system, thus introducing an artificial bias, to sample a smaller region (window) in the vicinity of a particular point on the reaction coordinate. The weighted histogram analysis method (WHAM)[23,24] was then used for combining the simulations done with different biasing (umbrella) potentials to extract the unbiased PMF from the biased

DOI: 10.1021/acs.jpcb.8b12088
J. Phys. Chem. B 2019, 123, 2679−2686

probability distributions and, hence, the free energy change along the reaction coordinate.

As an alternative to direct protonation of C2 by LYS175, we also considered the possibility of protonation via the classical Grotthuss mechanism.[25] In this mechanism, the charge from an excess proton can be effectively translocated along a network of H-bonded water molecules by a sequence of the so-called Grotthuss shuttling (or hopping) of protons between adjacent water molecules (giving rise to the concept of water wires). The Grotthuss mechanism has been implicated in various biological processes involving proton transport, including enzyme catalysis.[26−31] Here, the proton transfer to C2 would thus need to be assisted by at least one water molecule. In fact, examination of the crystal structure[12] reveals that binding of the RuBP phosphates is associated with a significant number of water molecules, one of which is suitably positioned for mediating the transfer of a proton from the P1 phosphate (upper 3PGA) to C2. However, no such structural water can be associated with proton transfer from LYS175. In addition, it should be noted that lysine with a typical pK_a of 10.5 is less likely to give up its proton to a water molecule compared with protonated phosphate ($-PO_3H^-$) with pK_a of around 7. For a Grotthuss mechanism with protonation at P1, we performed MEP calculations at the B3LYP/6-31G* level only due to the computational cost of additional PMF calculations.

Although the limitations of the B3LYP/6-31G* functional have been documented,[32,33] the present AIMD calculations are only made feasible by the modest size of the 6-31G* basis set. However, simple corrections may be applied to B3LYP/6-31G* to obtain B3LYP-gCP-D3/6-31G* energies,[34] which take into account the basis set superposition errors (BSSE) encountered when using 6-31G* (geometry counterpoise correction, gCP)[35] and the lack of long-range correlation (London dispersion correction, D3)[36,37] in B3LYP. As it cannot be easily incorporated into the NWChem calculations of energy gradients performed here, and, hence, the PMF calculations, we have used B3LYP-gCP-D3/6-31G* to obtain a more reliable estimate of the MEP only. Another source of uncertainty in the use of DFT stems from the plethora of semiempirical exchange−correlation functionals. However, functionals can be graded into generalized gradient approximation (GGA), meta-GGA, and their hybrid (incorporating exact Hartree−Fock exchange) variants, thereby facilitating meaningful comparisons.[38] Thus, rather than relying on energy estimation based on one type of functional (i.e., B3LYP form hybrid GGA), at critical points on the B3LYP/6-31G* MEP, we utilized a number of functionals drawn from each of the GGA, hybrid GGA, and hybrid meta-GGA taxonomies.

RESULTS

Direct Protonation from LYS175. *Energy-Minimized Surface.* The contour plot of the B3LYP/6-31G* energy-minimized surface (i.e., the energy at 0 K) is shown in Figure 3 (using Figure S1 data in the Supporting Information). From this potential energy surface, it is clear that the reaction is highly asymmetric with respect to changes in C2−C3 and C2−H distances. Transfer of the proton leading to the formation of products can only occur following the complete scission of the C2−C3 bond in the gemdiolate intermediate complex. Furthermore, as C2−C3 scission leads to an unstable carbanion intermediate, the reaction is concerted, i.e., scission and transfer must occur at the same time. The activation

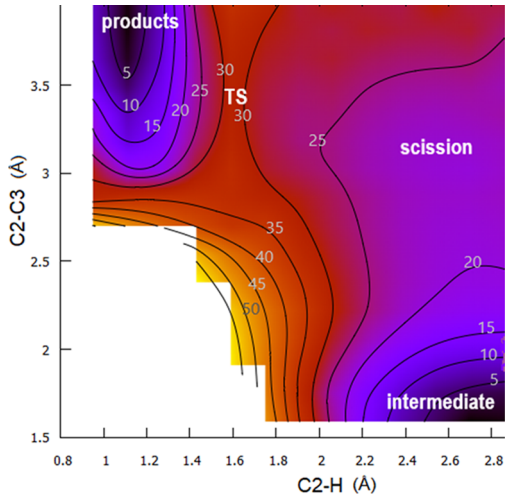

Figure 3. Energy (kcal/mol) contour surface at 0 K (minimum energy surface) for LYS175 proton donor as a function of C2−C3 and C2−H distances obtained from the interpolation of grid points (Figure S1 in the Supporting Information) optimized at the B3LYP/6-31G* level.

energy required to form product is the sum of the C2−C3 bond-scission energy (∼20 kcal/mol) plus the additional energy barrier (∼15 kcal/mol) to reach the transition state for transfer of the proton to C2, yielding a total activation energy of ∼35 kcal/mol for the combined sequential steps.

MEP and PMF. The B3LYP/6-31G* and corrected (B3LYP-gCP-D3/6-31G*) energies (relative to the intermediate) for the 27 grid points that trace the minimum B3LYP/6-31G* energy path from intermediate to products are given in Table 1. To facilitate comparison between the MEP and PMF energies, we have also defined a reaction coordinate as the difference between the C2−C3 and C2−H distances. This reaction coordinate for graphing the PMF calculations was obtained using the trend lines from plots of the mean values of the unbiased coordinate (C2−C3 or C2−H) in the MD as a function of the biased coordinate, as shown in Figure 4A,B. In Figure 4C, the C2−H(N) and C2−N(H) distances are plotted as a function of this reaction coordinate (RC). Initially, the mean distance between C2 and the lysine proton [H(N)] is 3 Å, close enough for direct transfer of the proton to C2. The difference between the two curves (∼1 Å, indicating C2−H−N are co-linear) reveals that the proton stays bonded to N of LYS175 side chain until after the TS state and product are formed. Although a single primitive (C2−H distance) is used to describe the proton transfer, the LYS175 side chain and upper 3PGA are able to move closer together, until close enough for the proton transfer, after which the distance increases.

Beginning with the intermediate state, the biased potential (umbrella sampling) was first applied to C2−C3 and then switched to C2−H in the bond-scission region to complete the formation of products. The MEP and PMF plotted as a function of the reaction coordinate (i.e., difference between the C2−C3 and H−C2 distances) are shown in Figure 5 (together with the B3LYP/6-31G* Grotthuss mechanism MEP for comparison). Overall, the thermodynamics does not favor the stereospecific transfer of a proton from the lysine (LYS175) side chain to C2, the free energy (PMF) of the product state being 5 kcal/mol higher than that of the gemdiolate intermediate. For the proton transfer, the PMF deviates

DOI: 10.1021/acs.jpcb.8b12088
J. Phys. Chem. B 2019, 123, 2679−2686

Table 1. Sequence of 27 Grid Points Defining the MEP Connecting Intermediate (2), Scission Region (8−14), TS (20), and Products (26) on the 2D Surface (Figure 3)[a]

	C2−C3 (Å)	C2−H (Å)	RC (Å)	B3LYP[b]	B3LYP[c]
1	1.43	2.70	−1.27	6.61	5.23
2	1.59	2.70	−1.11	0.00	0.00
3	1.75	2.70	−0.95	3.41	2.03
4	1.75	2.54	−0.79	5.37	4.17
5	1.75	2.38	−0.64	9.17	8.25
6	1.91	2.38	−0.48	13.52	12.20
7	2.06	2.38	−0.32	18.14	15.87
8	2.22	2.38	−0.16	21.57	18.78
9	2.38	2.38	0.00	22.24	19.32
10	2.54	2.38	0.16	22.14	19.25
11	2.70	2.38	0.32	22.00	19.06
12	2.86	2.38	0.48	22.09	19.05
13	3.02	2.38	0.64	21.43	18.63
14	3.18	2.38	0.79	21.44	19.07
15	3.18	2.22	0.95	22.78	20.67
16	3.18	2.06	1.11	24.83	22.67
17	3.18	1.91	1.27	25.03	24.18
18	3.33	1.91	1.43	25.30	23.53
19	3.33	1.75	1.59	27.36	26.37
20	3.33	1.59	1.75	31.02	30.03
21	3.33	1.43	1.91	23.97	20.83
22	3.33	1.27	2.06	23.41	21.21
23	3.49	1.27	2.22	11.61	7.75
24	3.49	1.11	2.38	3.91	0.37
25	3.65	1.11	2.54	1.08	−2.52
26	3.81	1.11	2.70	0.28	−3.38
27	3.81	0.95	2.86	8.83	5.60

[a]A reaction coordinate (RC), defined as the difference between C2−C3 and C2−H distances, was used (Figure 4) to plot the B3LYP and B3LYP-gCP-D3 energies (kcal/mol) relative to the intermediate. [b]B3LYP/6-31G*. [c]B3LYP-gCP-3D/6-31G*.

significantly from the MEP. However, the MEP is a reasonably good approximation to the PMF for the coordinate describing the C2−C3 bond scission.

BSSE and Dispersion Corrections. The B3LYP-gCP-D3/6-31G* (gCP-D3) energies deviate from the B3LYP/6-31G* energies at two critical points on the MEP (Table 1 and Figure 5). First, the B3LYP/6-31G* C2−C3 bond-dissociation energy of 22 kcal/mol reduces to 19 kcal/mol with the gCP-D3 correction; second, the B3LYP/6-31G* energy difference between the product and intermediate minima of 0.3 kcal/mol reduces to −3.4 kcal/mol. The total reduction amounts to only 1 kcal/mol at the TS. The BSSE (gCP) and dispersion (D3) components as a function of the reaction coordinate (RC) are given in Figure 6. Note that BSSE always overestimates the stabilization of a complex and so the correction is always a positive number, whereas dispersion (a correlation effect) must always work in the opposite direction, adding stabilization and so a negative contribution to the correction (Figure 6A). The DFT methods are more reliable in situations when these two effects cancel, otherwise both must be considered.[27,34] Relative to the intermediate state (Figure 6B), both BSSE and dispersion energy decrease along the RC, resulting in a decrease and increase, respectively, in the MEP, with the BSSE having the greater effect leading to an overall decrease in the MEP.

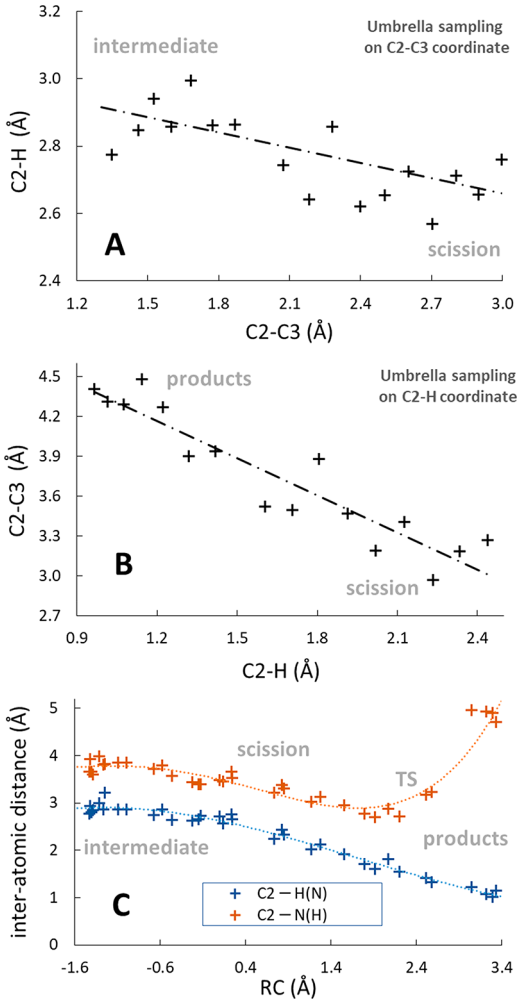

Figure 4. Mean values of the unbiased C2−C3 coordinate (A) and C2−H coordinate (B) in the MD (LYS175 proton donor) plotted as a function of the corresponding mean values of the biased coordinate (C2−H or C2−C3). The reaction coordinate (RC) used to graph the PMD in Figure 5 was determined from the trend lines (Figure S4, Supporting Information). Mean values of the C2−H and C2−N(H) distances (C) are plotted as functions of the RC derived from (A) and (B).

Exchange−Correlation Functionals. The results of single-point calculations (at the B3LYP/6-31G* optimized geometries) using various functionals are summarized in the Supporting Information (Figure S5). For a wide range of functionals, B3LYP predicts the lowest activation barrier for the proton transfer and the highest product energy. There is a strong linear correlation between activation barrier and energy of product formation.

Grotthuss Mechanism. *MEP.* The MEP for the Grotthuss mechanism is shown in Figure 5. As in direct protonation from LYS175, the overall reaction is concerted and highly asymmetrical, with proton transfer to the unstable C2 carbanion following scission of the C2−C3 bond in the gemdiolate intermediate. The reaction energy is exothermic (−14 kcal/mol at B3LYP/6-31G* level). The activation energy for scission of the C2−C3 bond and for the overall reaction is 13.6 kcal/mol. After scission is complete, the activation energy required for proton transfer to the C2 carbanion is minimal. As illustrated in Figure 7 (3PGA pathway), the proton from the water is transferred to C2 concerted with transfer of the excess

DOI: 10.1021/acs.jpcb.8b12088
J. Phys. Chem. B 2019, 123, 2679−2686

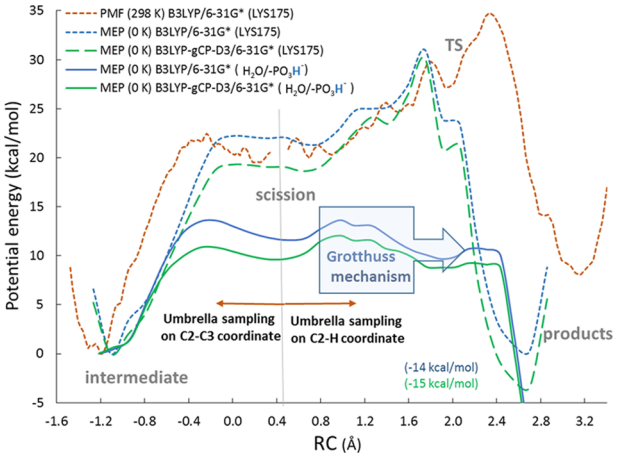

Figure 5. MEP (0 K) and PMF (298 K) plotted against the reaction coordinate (RC) defined as the difference between C2−C3 and C2−H distances (from Table 1 for the MEP and Figure 4 for the PMF). The proton donor moiety for each reaction profile is indicated in parenthesis (either protonation directly from LYS175 or via the Grotthuss mechanism initiated by a highlighted (blue) phosphate proton and a single water molecule).

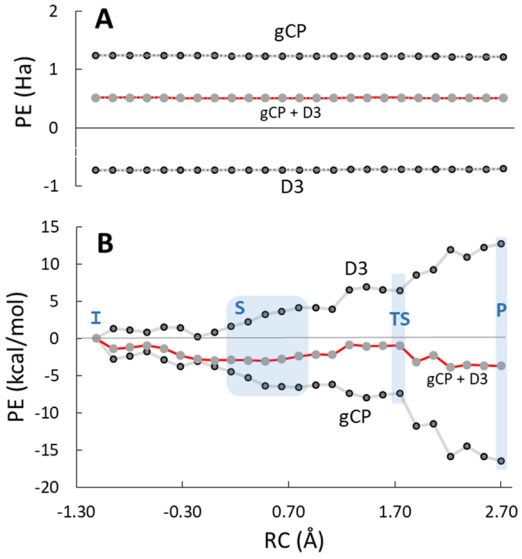

Figure 6. BSSE and dispersion correction for direct protonation by LYS175: (A) basis set superposition error (gCP) and dispersion correlation energy (D3) as a function of the reaction coordinate (RC). Note that any variations are not clearly visible on this energy scale. (B) Variation in gCP and D3 relative to the intermediate state (I): S = C2−C3 scission region, TS = C2−H transition state, P = final products. The red lines represent the sum total of the two corrections (gCP + D3) that must be applied to the B3LYP/6-31G* energies.

proton ("Grotthuss mechanism", Figure 5), leaving the 1-phosphate deprotonated. Moreover, the formation of pyruvate by β-elimination of phosphate, a side product of the reaction (see Discussion), can also be satisfactorily explained by a Grotthuss mechanism (Figure 7, pyruvate pathway).

BSSE and Dispersion Corrections. The results are qualitatively similar to direct protonation by LYS175. The gCP-D3 corrections when added to the B3LYP/6-31G* energies result in a lowering of the MEP (Figure 5). The maximum in the bond dissociation energy of 13.5 kcal/mol reduces to 10.8 kcal/mol with gCP-D3 correction. The energy

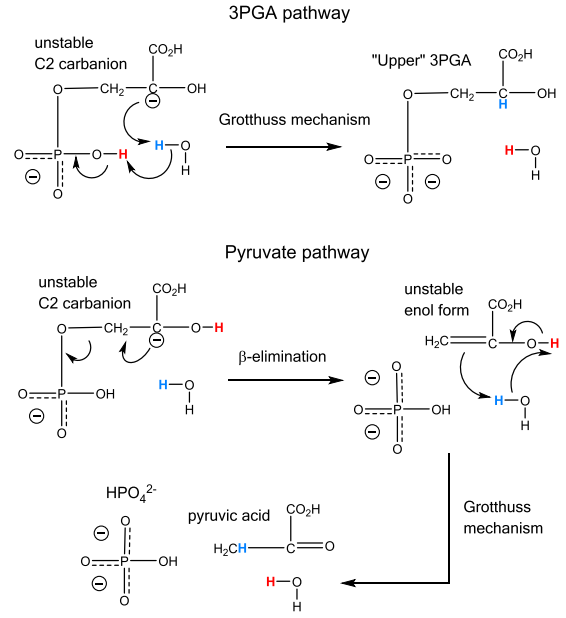

Figure 7. Grotthuss mechanism for the stereospecific C2 protonation step in the carboxylation reaction. In wild-type Rubisco, the main product formed is 3PGA. The production of pyruvic acid by elimination of phosphate, may also be explained by the Grotthuss mechanism.

difference between the product and intermediate minima of −14 kcal/mol reduces to −15 kcal/mol.

Exchange−Correlation Functionals. The mean and range of activation energies obtained from functionals classified according to GGA, hybrid GGA, and hybrid meta-GGA are presented in Figure 8; values for the individual functionals are

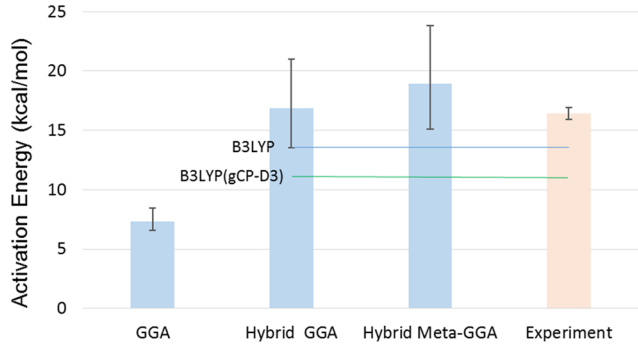

Figure 8. Mean values and range (error bars) of the activation energy for C2−C3 bond scission on the Grotthuss mechanism pathway (Figure 5) obtained from various DFT/6-31G* calculations (GGA, hybrid GGA, and hybrid meta-GGA) compared with the experimental activation (free) energy for carboxylation. B3LYP/B3LYP(gCP-D3) gives the lowest activation energy of the hybrid GGA class.

provided in the Supporting Information (Figure S6). The experimental result (Figure 8) was calculated from a range of observed catalytic rate constants.[1] The least-rated functionals (GGA) significantly underestimate the activation energy. The inclusion of Hartree−Fock exchange (hybrid GGA) greatly improves the mean estimate (B3LYP at the lower end). However, BSSE and dispersion corrections would lower the estimate (based on the B3LYP results). For the highest-rated class of functional (hybrid meta-GGA), the mean agreement with experiment is expected to be very close if BSSE and

DOI: 10.1021/acs.jpcb.8b12088
J. Phys. Chem. B 2019, 123, 2679−2686

dispersion corrections were to be included (as estimated from the B3LYP results). Thus, the hierarchy of functionals sampled exhibits convergence close to the experimental result.

DISCUSSION

The rate constant for turnover of product (k_{cat}) is limited partly by enolization of the RuBP prior to binding CO_2 or O_2,[39−41] and partly by the subsequent C3 hydration, scission of the C2−C3 bond, and C2 protonation (co-limitation), although it has not been determined experimentally which one of these is limiting or whether sequential or concerted steps are involved.[42] However, in light of the results of the present computational study, C2 cannot be protonated by LYS175, both on thermodynamic and kinetic grounds. As the activation barrier of 35 kcal/mol calculated here (Figure 5) for the LYS175 donor is significantly higher than the experimental activation free energy of 16 kcal/mol (corresponding to k_{cat}),[1,43] this conclusion is not likely to change if other computational methodologies[31,44] were adopted, quantum dynamic effects[45−47] included, or alternative DFT functional used (see also Figure S5 in the Supporting Information). This is in stark contrast to the Grotthuss mechanism, which predicts an activation energy in excellent agreement with the experiment (Figure 8). In addition, given that the PMF for a proton transfer (Figure 5) suggests that the product enthalpy is likely far less exothermic than estimated by the MEP, the Grotthuss mechanism is broadly consistent with the observed reaction enthalpy.[48] The activation energy is dominated by scission of the C2−C3 bond and modulated by the stereospecific C2 protonation in a concerted but highly asymmetric reaction step. The present results, together with those obtained previously,[6] demonstrate that double protonation of the upper 3PGA (at both carboxylate and 1-phosphate) are sufficient to reduce the C2−C3 bond-scission energy to the level required for the reaction to proceed. In the absence of any other active-site proton donors, an alternative source for these protons might be provided from the presence of "water wires"[49−51] connecting solvent with the enzyme active site. Site-directed mutagenesis and the kinetic isotope effect are experimental tools commonly used to study enzyme catalysis. The experimental evidence for Rubisco is consistent with protonation facilitated by water, as discussed below.

Site-Directed Mutagenesis. Pyruvate is a known by-product (derived from β-elimination of the intermediate, i.e., cleavage of the carbon−phosphate bond in the upper 3PGA) that competes with 3PGA production in the carboxylation reaction.[52,53] The K175G (lysine to glycine) mutant produces pyruvate rather than 3PGA,[53] suggesting that the forward processing of the intermediate (gemdiolate) to product does not require that lysine donate a proton (assuming that β-elimination also requires protonation). This confirms that LYS175 is necessary for the efficient production of 3PGA but not necessarily the actual source of the final proton in the wild-type Rubisco. The K175G mutant results do not preclude the possibility that the final protonation in wild-type Rubisco comes from a source other than LYS175. The source of the proton that yields the final product (either pyruvate in the mutant or 3PGA in the wild type) thus remains uncertain. Clearly, any proposals for the protonation mechanism must be able to explain the formation of both (pyruvate and 3PGA) products (Figure 7).

Deuterium Isotope Effects. The observed deuterium isotope effects (DIEs) on Rubisco kinetic parameters (k_{cat} and K_m (i.e., K_C for carboxylation) from spinach Rubisco) demonstrate the exchange of protons between the active site and solvent occurs at various steps of the reaction.[43] There is an observable deuterium isotope effect (DIE) of 1.75 on the k_{cat} for carboxylation. Formation of a stable C2 carbanion intermediate by scission of the C2−C3 bond would not be expected to contribute to the DIE if no protons are involved, and accordingly the DIE would be attributable to enolization (the co-limiting step) alone. However, a post-enolization contribution to the DIE would be consistent with a protonation role associated with the bond scission. In addition, increasing the mole fraction of D_2O increases the production of pyruvate, suggesting a slowing of the C2-protonation rate, thus permitting greater β-elimination. This provides further evidence that a proton from the solvent is involved in a rate-limiting step. The larger corresponding DIE for oxygenation (1.97) may reflect the involvement of more than one proton in the bond-scission transition state, as the formation of the upper product (2PG instead of 3PGA) requires protonation and elimination of water.

CONCLUSIONS

Although PMF calculations using WHAM are readily extendable to multidimensional reaction coordinates,[23] many more MD simulations are required to complete the free energy surface, which can become prohibitive for model systems of the size (343 atoms) used in the present study (Figure 2), particularly when MD is carried out with a force field grounded in the Kohn−Sham DFT for the calculation of the electronic energy. However, assuming the energy-minimized surface (0 K) gives a reasonably accurate a priori representation of the corresponding free-energy surface, umbrella sampling may be restricted to the vicinity of the MEP requiring far fewer AIMD simulations. Using this approach, we found that a final reaction step involving stereospecific transfer of the proton from a conserved active-site lysine (LYS175 in spinach Rubisco) to C2 is more accurately described by the PMF (298 K), rather than the MEP (0 K), whereas the MEP was found to be a reasonably good approximation to the PMF for the coordinate describing the C2−C3 bond scission. Furthermore, BSSE corrections were also found to be of some significance. Consistent with the experimental findings that suggest LYS175 is not required for product formation, the overall result casts considerable doubt as to whether this conserved lysine is the donor in the stereospecific protonation of C2 in the final step of the reaction. Alternatively, a Grotthuss mechanism, involving one water molecule and an excess proton positioned at the P1 phosphate of RuBP, is consistent with the experimental observations of activation energy, reaction enthalpy, site-directed mutagenesis, and deuterium isotope effects.

ASSOCIATED CONTENT

Supporting Information

The Supporting Information is available free of charge on the ACS Publications website at DOI: 10.1021/acs.jpcb.8b12088.

Calculations and results used to generate minimum energy potential energy surface (Figure S1); MD calculation and results of umbrella sampling on C2−C3 and C2−H coordinates (Figure S2); normalized probability distributions from umbrella sampling (Figure S3); output of PMF calculations with listing of computer

DOI: 10.1021/acs.jpcb.8b12088
J. Phys. Chem. B 2019, 123, 2679−2686

code (Figure S4); results of single-point calculations of activation energy comparing B3LYP with other DFT methods (Figures S5 and S6) (PDF)

AUTHOR INFORMATION

Corresponding Author

*E-mail: peter.cummins@anu.edu.au.

ORCID

Peter L. Cummins: 0000-0003-3096-6634

Babu Kannappan: 0000-0001-8148-8834

Notes

The authors declare no competing financial interest.

ACKNOWLEDGMENTS

This research was undertaken with the assistance of resources and services from the National Computational Infrastructure (NCI), which is supported by the Australian Government. We thank the reviewers for helpful suggestions.

REFERENCES

(1) Cummins, P. L.; Kannappan, B.; Gready, J. E. Directions for Optimization of Photosynthetic Carbon Fixation: RuBisCO's Efficiency May Not Be So Constrained After All. *Front. Plant Sci.* **2018**, *9*, 183.

(2) Gready, J. E.; Kannappan, B. Process for Generation of Protein and Uses Thereof. U.S. Patent US12/422190, 2017.

(3) Harpel, M. R.; Larimer, F. W.; Hartman, F. C. Multifaceted Roles of Lys166 of Ribulose-Bisphosphate Carboxylase/Oxygenase as Discerned by Product Analysis and Chemical Rescue of Site-Directed Mutants. *Biochemistry* **2002**, *41*, 1390−1397.

(4) Taylor, T. C.; Andersson, I. Structure of a Product Complex of Spinach Ribulose-1,5-Bisphosphate Carboxylase/Oxygenase. *Biochemistry* **1997**, *36*, 4041−4046.

(5) Cleland, W. W.; Andrews, T. J.; Gutteridge, S.; Hartmann, F. C.; Lorimer, G. H. Mechanism of Rubisco: The Carbamate as General Base. *Chem. Rev.* **1998**, *98*, 549−562.

(6) Cummins, P. L.; Kannappan, B.; Gready, J. E. Revised Mechanism of Carboxylation of Ribulose-1,5-Biphosphate by Rubisco from Large Scale Quantum Chemical Calculations. *J. Comput. Chem.* **2018**, *39*, 1656−1665.

(7) King, W. A.; Gready, J. E.; Andrews, T. J. Quantum Chemical Analysis of the Enolization of Ribulose Bisphosphate: The First Hurdle in the Fixation of CO_2 by Rubisco. *Biochemistry* **1998**, *37*, 15414−15422.

(8) Mauser, H.; King, W. A.; Gready, J. E.; Andrews, T. J. CO_2 Fixation by Rubisco: Computational Dissection of the Key Steps of Carboxylation, Hydration, and C-C Bond Cleavage. *J. Am. Chem. Soc.* **2001**, *123*, 10821−10829.

(9) Kannappan, B.; Gready, J. E. Redefinition of Rubisco Carboxylase Reaction Reveals Origin of Water for Hydration and New Roles for Active-Site Residues. *J. Am. Chem. Soc.* **2008**, *130*, 15063−15080.

(10) Mezei, M.; Beveridge, D. L. Free Energy Simulations. *Ann. N. Y. Acad. Sci.* **1986**, *482*, 1−24.

(11) Kohn, W.; Sham, L. J. Self-Consistent Equations Including Exchange and Correlation Effects. *Phys. Rev.* **1965**, *140*, A1133−A1138.

(12) Andersson, I. Large Structures at High Resolution: The 1.6 Å Crystal Structure of Spinach Ribulose-1,5-Bisphosphate Carboxylase/Oxygenase Complexed with 2-Carboxyarabinitol Bisphosphate. *J. Mol. Biol.* **1996**, *259*, 160−74.

(13) Becke, A. D. Density-functional thermochemistry. III. The role of exact exchange. *J. Chem. Phys.* **1993**, *98*, 5648−5652.

(14) Lee, C.; Yang, W. T.; Parr, R. G. Development of the Colle-Salvetti Correlation-Energy Formula into a Functional of the Electron Density. *Phys. Rev. B* **1988**, *37*, 785−789.

(15) Vosko, S. H.; Wilk, L.; Nusair, M. Accurate Spin-Dependent Electron Liquid Correlation Energies for Local Spin Density Calculations: a Critical Analysis. *Can. J. Phys.* **1980**, *58*, 1200−1211.

(16) Hariharan, P. C.; Pople, J. A. The Influence of Polarization Functions on Molecular Orbital Hydrogenation Energies. *Theor. Chim. Acta* **1973**, *28*, 213−222.

(17) Marx, D.; Hutter, J. *Ab Initio Molecular Dynamics: Basic Theory and Advanced Methods*; Cambridge University Press: Cambridge, U.K., 2009.

(18) Valiev, M.; Bylaska, E. J.; Govind, N.; Kowalski, K.; Straatsma, T. P.; van Dam, H. J. J.; Wang, D.; Nieplocha, J.; Apra, E.; Windus, T. L.; de Jong, W. A. NWChem: A Comprehensive and Scalable Open-Source Solution for Large Scale Molecular Simulations. *Comput. Phys. Commun.* **2010**, *181*, 1477−1489.

(19) Verlet, L. Computer "Experiments" on Classical Fluids. I. Thermodynamical Properties of Lennard-Jones Molecules. *Phys. Rev.* **1967**, *159*, 98−103.

(20) Swope, W. C.; Anderson, H. C.; Berens, P. H.; Wilson, K. R. A Computer Simulation Method for the Calculation of Equilibrium Constants for the Formation of Physical Clusters of Molecules: Application to Small Water Clusters. *J. Chem. Phys.* **1982**, *76*, 637−649.

(21) Bussi, G.; Donadio, D.; Parrinello, M. Canonical Sampling Through Velocity Rescaling. *J. Chem. Phys.* **2007**, *126*, No. 014101.

(22) Torrie, G. M.; Valleau, J. P. Monte Carlo Free Energy Estimates using non-Boltzmann Sampling: Application to the Sub-Critical Lennard-Jones Fluid. *Chem. Phys. Lett.* **1974**, *28*, 578−581.

(23) Kumar, S.; Rosenberg, J. M.; Bouzida, D.; Swendsen, R. H.; Kollman, P. A. The Weighted Histogram Analysis Method for Free-Energy Calculations on Biomolecules. I. The Method. *J. Comput. Chem.* **1992**, *13*, 1011−1021.

(24) Roux, B. The Calculation of the Potential of Mean Force using Computer Simulations. *Comput. Phys. Commun.* **1995**, *91*, 275−282.

(25) Agmon, N. The Grotthuss mechanism. *Chem. Phys. Lett.* **1995**, *244*, 456−462.

(26) Swanson, J. M. J.; Maupin, C. M.; Chen, H.; Petersen, M. K.; Xu, J.; Wu, Y.; Voth, G. A. Proton Solvation and Transport in Aqueous and Biomolecular Systems: Insights from Computer Simulations. *J. Phys. Chem. B* **2007**, *111*, 4300−4314.

(27) Bjerregaard-Andersen, K.; Sommer, T.; Jensen, J. K.; Jochimsen, B.; Etzerodt, M.; Morth, J. P. A Proton Wire and Water Channel Revealed in the Crystal Structure of Isatin Hydrolase. *J. Biol. Chem.* **2014**, *289*, 21351−21359.

(28) Bekçioğlu, G.; Allolio, C.; Sebastiani, D. Water Wires in Aqueous Solutions from First-Principles Calculations. *J. Phys. Chem. B* **2015**, *119*, 4053−4060.

(29) Szabla, R.; Sponer, J.; Gora, R. W. Electron-Driven Proton Transfer Along H_2O Wires Enables Photorelaxation of $\pi\sigma^*$ States in Chromophore−Water Clusters. *J. Phys. Chem. Lett.* **2015**, *6*, 1467−1471.

(30) Miyake, T.; Rolandi, M. Grotthuss Mechanisms: From Proton Transport in Proton Wires to Bioprotonic Devices. *J. Phys.: Condens. Matter* **2016**, *28*, No. 023001.

(31) Paul, S.; Paul, T. K.; Taraphder, S. Reaction Coordinate, Free Energy, and Rate of Intramolecular Proton Transfer in Human Carbonic Anhydrase II. *J. Phys. Chem. B* **2018**, *122*, 2851−2866.

(32) Zhao, Y.; Truhlar, D. G. Density Functionals with Broad Applicability in Chemistry. *Acc. Chem. Res.* **2008**, *41*, 157−167.

(33) Goerigk, L.; Kruse, H.; Grimme, S. Benchmarking Density Functional Methods against the S66 and S66x8 Datasets for non-Covalent Interactions. *ChemPhysChem* **2011**, *12*, 3421−3433.

(34) Kruse, H.; Goerigk, L.; Grimme, S. Why the Standard B3LYP/6-31G* Model Chemistry Should Not Be Used in DFT Calculations of Molecular Thermochemistry: Understanding and Correcting the Problem. *J. Org. Chem.* **2012**, *77*, 10824−10834.

(35) Kruse, H.; Grimme, S. A Geometrical Correction for the inter- and intra-Molecular Basis Set Superposition Error in Hartree-Fock and Density Functional Theory Calculations for Large Systems. *J. Chem. Phys.* **2012**, *136*, No. 154101.

DOI: 10.1021/acs.jpcb.8b12088
J. Phys. Chem. B 2019, 123, 2679−2686

(36) Grimme, S.; Antony, J.; Ehrlich, S.; Krieg, H. A Consistent and Accurate Ab Initio Parametrization of Density Functional Dispersion Correction (DFT-D) for the 94 Elements H-Pu. *J. Chem. Phys.* **2010**, *132*, No. 154104.
(37) Grimme, S.; Ehrlich, S.; Goerigk, L. Effect of the Damping Function in Dispersion Corrected Density Functional Theory. *J. Comput. Chem.* **2011**, *32*, 1456−1465.
(38) Perdew, J. P.; Ruzsinszky, A.; Tao, J.; Staroverov, V. N.; Scuseria, G. E.; Csonka, G. I. Prescription for the Design and Selection of Density Functional Approximations: More Constraint Satisfaction with Fewer Fits. *J. Chem. Phys.* **2005**, *123*, No. 062201.
(39) Sue, J. M.; Knowles, J. R. Ribulose 1,5-Bisphosphate Carboxylase: Primary Deuterium Kinetic Isotope Effect using [3-2H]Ribulose 1,5-Bisphosphate. *Biochemistry* **1982**, *21*, 5410−5414.
(40) Saver, B. G.; Knowles, J. R. Ribulose 1,5-Bisphosphate Carboxylase: Enzyme-Catalyzed Appearance of Solvent Tritium at Carbon 3 of Ribulose 1,5-Bisphosphate Reisolated after Partial Reaction. *Biochemistry* **1982**, *21*, 5398−5403.
(41) Van Dyk, D. E.; Schloss, J. V. Deuterium Isotope Effects in the Carboxylase Reaction of Ribulose-1,5-Bisphosphate Carboxylase/Oxygenase. *Biochemistry* **1986**, *25*, 5145−5156.
(42) Tcherkez, G. G. B.; Bathellier, C.; Stuart-Williams, H.; Whitney, S.; Gout, E.; Bligny, R.; Badger, M.; Farquhar, G. D. D_2O Solvent Isotope Effects Suggest Uniform Energy Barriers in Ribulose-1,5-bisphosphate Carboxylase/Oxygenase Catalysis. *Biochemistry* **2013**, *52*, 869−877.
(43) McNevin, D.; von Caemmerer, S.; Farquhar, G. Determining RuBisCO Activation Kinetics and other Rate and Equilibrium Constants by Simultaneous Multiple Non-Linear Regression of a Kinetic Model. *J. Exp. Bot.* **2006**, *57*, 3883−3900.
(44) Schutz, C. N.; Warshel, A. Analyzing Free Energy Relationships for Proton Translocations in Enzymes: Carbonic Anhydrase Revisited. *J. Phys. Chem. B* **2004**, *108*, 2066−2075.
(45) Vardi-Kilshtain, A.; Nitoker, N.; Major, D. T. Nuclear Quantum Effects and Kinetic Isotope Effects in Enzyme Reactions. *Arch. Biochem. Biophys.* **2015**, *582*, 18−27.
(46) Wang, M.; Lu, Z.; Yang, W. Nuclear Quantum Effects on an Enzyme-Catalyzed Reaction with Reaction Path Potential: Proton Transfer in Triosephosphate Isomerase. *J. Chem. Phys.* **2006**, *124*, No. 124516.
(47) Sundar, V.; Gelbwaser-Klimovsky, D.; Aspuru-Guzik, A. Reproducing Quantum Probability Distributions at the Speed of Classical Dynamics: A New Approach for Developing Force-Field Functors. *J. Phys. Chem. Lett.* **2018**, *9*, 1721−1727.
(48) Frank, J.; Kositza, J. M.; Vater, J.; Holzwarth, J. F. Microcalorimetric Determination of the Reaction Enthalpy Changes Associated with the Carboxylase and Oxygenase Reactions Catalysed by Ribulose 1,5-Bisphosphate Carboxylase/Oxygenase (RUBISCO). *Phys. Chem. Chem. Phys.* **2000**, *2*, 1301−1304.
(49) Wraight, C. A. Chance and Design—Proton Transfer in Water, Channels and Bioenergetic Proteins. *Biochim. Biophys. Acta* **2006**, *1757*, 886−912.
(50) Kaila, V. I. R.; Hummer, G. Energetics and Dynamics of Proton Transfer Reactions along Short Water Wires. *Phys. Chem. Chem. Phys.* **2011**, *13*, 13207−13215.
(51) Peng, Y.; Swanson, J. M. J.; Kang, S.-G.; Zhou, R.; Voth, G. A. Hydrated Excess Protons can Create their Own Water Wires. *J. Phys. Chem. B* **2015**, *119*, 9212−9218.
(52) Lorimer, G. H.; Hartman, F. C. Evidence Supporting Lysine 166 of Rhodospirillum Rubrum Ribulosebisphosphate Carboxylase as the Essential Base Which Initiates Catalysis. *J. Biol. Chem.* **1988**, *263*, 6468−6471.
(53) Morell, M. K.; Wilkin, J.-M.; Kane, H. J.; Andrews, T. J. Side Reactions Catalyzed by Ribulose-bisphosphate Carboxylase in the Presence and Absence of Small Subunits. *J. Biol. Chem.* **1997**, *272*, 5445−5451.

DOI: 10.1021/acs.jpcb.8b12088
J. Phys. Chem. B 2019, 123, 2679−2686